

OSDFace: One-Step Diffusion Model for Face Restoration

Jingkai Wang^{1*}, Jue Gong^{1*}, Lin Zhang¹, Zheng Chen¹
Xing Liu², Hong Gu², Yutong Liu^{1†}, Yulun Zhang^{1†}, Xiaokang Yang¹
¹Shanghai Jiao Tong University, ²vivo Mobile Communication Co., Ltd

Abstract

Diffusion models have demonstrated impressive performance in face restoration. Yet, their multi-step inference process remains computationally intensive, limiting their applicability in real-world scenarios. Moreover, existing methods often struggle to generate face images that are harmonious, realistic, and consistent with the subject’s identity. In this work, we propose OSDFace, a novel one-step diffusion model for face restoration. Specifically, we propose a visual representation embedder (VRE) to better capture prior information and understand the input face. In VRE, low-quality faces are processed by a visual tokenizer and subsequently embedded with a vector-quantized dictionary to generate visual prompts. Additionally, we incorporate a facial identity loss derived from face recognition to further ensure identity consistency. We further employ a generative adversarial network (GAN) as a guidance model to encourage distribution alignment between the restored face and the ground truth. Experimental results demonstrate that OSDFace surpasses current state-of-the-art (SOTA) methods in both visual quality and quantitative metrics, generating high-fidelity, natural face images with high identity consistency. The code and model will be released at <https://github.com/jkwang28/OSDFace>.

1. Introduction

Face restoration aims to restore high-quality (HQ) face images from degraded low-quality (LQ) inputs caused by complex degradation processes. Blur, noise, downsampling, and JPEG compression are common degradation types that can significantly affect the quality of face images, leading to an ill-posed problem. Recent advancements focus on leveraging CNN-based methods and Transformer-based methods [51, 58, 61, 74] to restore HQ face images, and have shown remarkable performance. However, due to the severe degradation of face images, generative models with strong prior knowledge exhibit irreplaceable advantages.

Generative adversarial networks (GANs) [14] and dif-

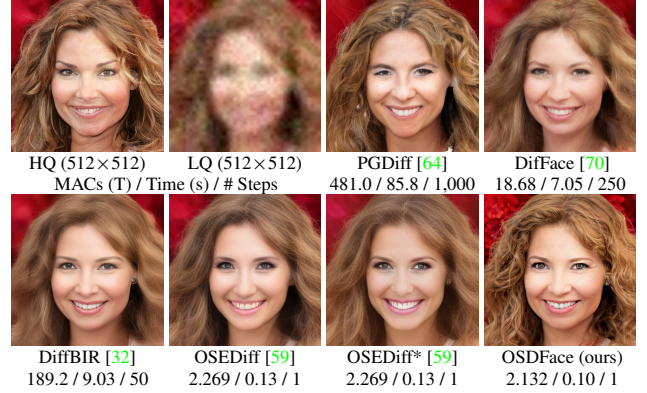


Figure 1. Visual samples of diffusion-based face restoration methods. We provide multiply-accumulate operations (MACs), time, and number of timesteps during inference. Our OSDFace achieves a more natural and faithful visual result than other ones.

fusion models [18, 46, 47] have gained considerable attention for generating high-fidelity images with perceptual details. Many efforts, such as DiffFace [70] and DiffBIR [32], have also been applied to restoring HQ face images [3, 6, 7, 36, 38, 49, 54, 64, 66]. However, GANs are challenging to train and may encounter issues such as mode collapse and training instability. Conversely, diffusion models produce promising results but require multiple forward passes during inference, leading to increased computational cost and longer inference time.

To speed up the diffusion inference, one-step diffusion (OSD) models [28, 59] have emerged as a promising research topic. Benefiting from the recently developed generative diffusion models, especially large-scale pretrained text-to-image (T2I) models [40, 41], OSD models [28, 59] enjoy the powerful restoration capability and fast inference speed. It is anticipated that OSD models could be highly competitive in face restoration practical applications.

As shown in Fig. 1, most diffusion-based face restoration methods can effectively recover basic facial features such as eyes, mouth, and contour. However, details, such as realistic-looking hair and complex backgrounds, often remain unharmonious. The primary issue lies in the insufficient incorporation of face priors [62]. Some diffusion-based methods [7, 32, 70] rely solely on the diffusion

*Equal contribution.

†Corresponding authors.

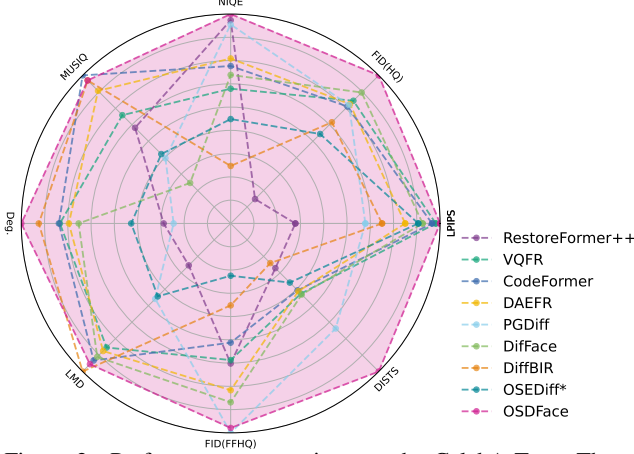


Figure 2. Performance comparison on the CelebA-Test. Those metrics which smaller scores indicate better image quality, are inverted and normalized for display. OSDFace achieves leading scores on most metrics with only one diffusion step.

model without considering face priors, resulting in unrealistic restorations. Other methods [49, 64] attempt to use face priors, but either limit the generative capabilities or cause information reduction. On the other hand, existing general OSD image restoration models, such as OSediff [59], are not specifically designed for facial features. OSediff employs image-to-tag prior and works well for natural images. However, it meets challenges when applied to faces, as humans are highly sensitive to facial features, and even minor inconsistencies or unrealistic details are easily noticeable.

Thus, it is worthwhile to investigate how to design a prior capturer and apply it to OSD model. **One key issue is that** designing priors to capture rich facial features is challenging. Vector-quantized (VQ) prior-based methods, such as CodeFormer [74] and DAEFR [51], effectively leverage codebooks trained in HQ data as priors for face restoration. These models perform well in generating facial features. However, the face images often lack fine details and display unreal backgrounds because they are generated by the codebook items directly. **Furthermore**, incorporating priors into diffusion models for face restoration is also a critical focus. Numerous efforts have been undertaken to incorporate face priors. For example, PGDiff [64] employs a face prior by pretraining a VQ-based restorer and using it as a target to guide the diffusion model. Due to limitations imposed by the target model, such a configuration inhibits the generative capabilities. In addition, CLRFace [49] passes denoised latent vectors to a pretrained codebook and a subsequent decoder. Relying on direct image generation with a fixed-size codebook limits the diversity of results.

To alleviate the limitations, we propose a novel method, OSDFace, for face restoration. **Firstly**, OSDFace is an OSD model that leverages the powerful image restoration capabilities of diffusion models, as shown in Fig. 2, while offering a fast inference speed (about 0.1s for a 512×512 image).

Secondly, our OSDFace integrates a visual representation embedder (VRE) to extract rich facial information directly from LQ inputs. Our proposed VRE consists of two components: a visual tokenizer and a VQ embedder. The visual tokenizer contains a VAE encoder and a VQ dictionary matching function. Trained on LQ data, it could efficiently capture information from LQ faces. In the same LQ semantic space, the VQ embedder performs a dictionary lookup of feature categories to obtain the visual prompt in $\mathcal{O}(1)$ time. **Thirdly**, to better keep a consistent identity, we incorporate a facial identity loss derived from face recognition into our training process. This approach significantly reduces the distance between the generated faces and the ground truth in the compact deep feature space. Besides, we employ a GAN discriminator as a guidance model, which encourages the distribution alignment between the generated faces and the ground truth. The alignment enables the model suitable for faces in complex environments.

Our contributions can be summarized as follows.

- We propose OSDFace, a novel and effective one-step diffusion model for face restoration. This is the first attempt to utilize one-step diffusion for restoring faces.
- We design the visual representation embedder (VRE). Using LQ dictionary, VRE captures rich prior from LQ images for a deeper understanding of visual content.
- We customize a comprehensive method for realistic face alignment, incorporating facial identity loss for identity consistency and GAN loss for distribution alignment.
- Our OSDFace achieves significant SOTA face restoration performance, excelling in visual quality and quantitative metrics with reduced computational costs.

2. Related Work

2.1. Face Restoration

Face restoration aims to recover high-quality (HQ) faces from low-quality (LQ) inputs affected by complex degradations. A key challenge for researchers is how to grasp face prior efficiently and effectively. Statistical priors are widely used in traditional image processing techniques. Recently, with the development of deep learning, researchers have begun to explore more advanced learning-based methods.

Geometric priors [8, 26, 44, 69], while useful, are limited by the degree of degradation in low-quality images, restricting their ability to recover high-quality details. Reference priors [11, 29–31] aim to supplement missing information using the corresponding high-quality reference images. However, obtaining references that match the target data is often impractical. Generative priors [15, 35, 52, 54, 63] from pretrained models are widely used for face restoration. These priors are typically incorporated into encoder-decoder networks through iterative latent optimization or direct latent encoding to enhance fidelity. This approach has demonstrated stronger restoration potential compared to

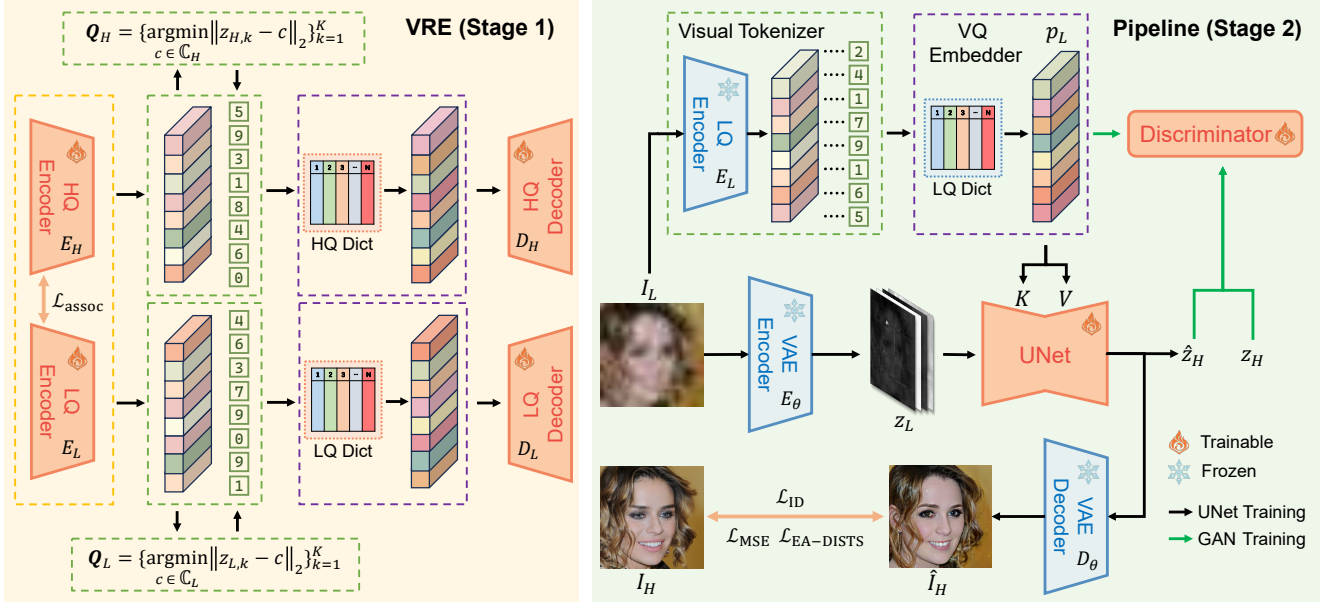


Figure 3. Training framework of OSDFace. **First**, to establish a visual representation embedder (VRE), we train the autoencoder and VQ dictionary for HQ and LQ face domains using self-reconstruction and feature association loss $\mathcal{L}_{\text{assoc}}$. **Then**, we use the VRE containing LQ encoder and dictionary to embed the LQ face I_L , producing the visual prompt embedding p_L . **Next**, the LQ image I_L along with p_L are inputted into the generator \mathcal{G}_θ to yield the predicted HQ face \hat{I}_H : $\hat{I}_H = \mathcal{G}_\theta(I_L; \text{VRE}(I_L))$. The generator \mathcal{G}_θ incorporates the pretrained VAE and UNet from Stable Diffusion, with only the UNet fine-tuned via LoRA. **Additionally**, a series of feature alignment losses are applied to ensure the generation of harmonious and coherent face images. The generator and discriminator are trained alternately.

earlier methods. Recently, diffusion priors [13, 24, 55, 64] have gained attention with advancements in diffusion models. The degraded images are generated from intermediate outputs at each diffusion iteration. In parallel, VQ prior-based methods [16, 51, 58, 74] have shown great promise, achieving impressive results in face restoration. They typically reconstruct images by matching features extracted from LQ inputs to items in a codebook, and then directly output the restored images. However, the limited capacity of VQ priors often leads to blurry backgrounds and unprecise details. Therefore, how to leverage face prior information more effectively remains a crucial problem.

2.2. Diffusion Models

Diffusion models, known for powerful generative capacity, transform random noise into structured data through iterative denoising processes. Moreover, diffusion models have achieved promising results in image restoration recently, showing strong performance in image-to-image tasks using efficient guidance strategies [7, 32, 36, 38, 49, 70]. However, some models possess highly complex structures [7, 49]. Most of them require numerous iterative steps, limiting their popularization for real-world applications.

Reducing the inference steps of diffusion models is critical to accelerating generation speeds and reducing computational costs. Yet, further reduction often results in a significant performance drop, making it crucial to balance inference speed with model capability. Most one-step dif-

fusion (OSD) methods employ distillation to learn from a teacher model, ensuring the quality of the generated images [56, 59, 67, 68]. D³SR [28] achieves promising results with OSD, free from the limitations of model distillation. However, all models are designed primarily for natural image restoration and lack strong generalization for face-specific tasks. It is essential to incorporate prior knowledge specific to human faces to enhance the applicability of OSD models in face restoration. Consequently, the models could generate more realistic and high-fidelity face images.

3. Method

We aim to extract as many features as possible from low-quality (LQ) source images. These features are used as prompts to guide the diffusion model in generating realistic faces that closely resemble the individuals in the original images. To accomplish this, we propose an innovative one-step diffusion model (see Fig. 3) focused on face restoration. This model enhances the realism of the generated faces while preserving the characteristics of LQ images.

3.1. One-Step Diffusion (OSD) Model

Latent diffusion models [40] are structured around both forward and reverse operations. During the forward diffusion phase, Gaussian noise with a variance $\beta_t \in (0, 1)$ is incrementally added to the latent vector z at each timestep, resulting in $z_t = \sqrt{\alpha_t} z + \sqrt{1 - \alpha_t} \varepsilon$, where $\varepsilon \sim \mathcal{N}(0, I)$. Here, α_t is defined as $1 - \beta_t$, and $\bar{\alpha}_t$ denotes the cumulative product of α_s up to timestep t : $\bar{\alpha}_t = \prod_{s=1}^t \alpha_s$.

In the reverse phase, the clean latent vector \hat{z}_0 can be estimated directly using the predicted noise $\hat{\varepsilon}$:

$$\hat{z}_0 = \frac{z_t - \sqrt{1 - \bar{\alpha}_t} \hat{\varepsilon}}{\sqrt{\bar{\alpha}_t}}. \quad (1)$$

The predicted noise $\hat{\varepsilon}$ could be formally expressed as $\varepsilon_\theta(z_t; p, t)$, where p denotes prompt embedding.

As illustrated in Fig. 3, we first employ the encoder E_θ to map the low-quality (LQ) image I_L into the latent space, yielding $z_L = E_\theta(I_L)$. Next, we perform one denoising step to obtain the predicted noise $\hat{\varepsilon}$, allowing us to compute the predicted high-quality (HQ) latent vector \hat{z}_H :

$$\hat{z}_H = \frac{z_L - \sqrt{1 - \bar{\alpha}_{T_L}} \varepsilon_\theta(z_L; p, T_L)}{\sqrt{\bar{\alpha}_{T_L}}}, \quad (2)$$

where ε_θ denotes the denoising network parameterized by θ , and T_L is the diffusion timestep.

Unlike one-step T2I diffusion models [48, 68], the UNet input in OSDFace is not entirely Gaussian noise. Therefore, we predefine a parameter $T_L \in [0, T]$ and feed it into the UNet, where T represents the total diffusion timesteps (in Stable Diffusion, T is set to 1,000). Finally, we use the decoder D_θ to reconstruct the HQ face \hat{I}_H from \hat{z}_H :

$$\hat{I}_H = D_\theta(\hat{z}_H). \quad (3)$$

Denoting the entire generator as \mathcal{G} , the overall computation procedure can be represented as:

$$\hat{I}_H = \mathcal{G}(I_L; p). \quad (4)$$

3.2. Stage 1. Visual Representation Embedder

Previous studies have emphasized the critical importance of understanding input images and integrating face prior into models. To incorporate priors, we first train a feature extraction module, *i.e.*, visual representation embedder (VRE), in stage 1 for LQ inputs. In stage 2, we utilize the pretrained VRE to guide the diffusion model, allowing it to leverage prior knowledge from the input image more effectively.

We design a variational autoencoder (VAE) with a vector-quantized (VQ) dictionary [12, 37] for effective feature extraction. The architecture consists of the VRE and a VAE decoder utilized exclusively during the first training stage. Through self-reconstruction training, the VRE builds a dictionary of image categories as priors, enabling it to act as a multi-class embedder using the VQ dictionary.

Given a low-quality (LQ) face $I_L \in \mathbb{R}^{H \times W \times 3}$, the encoder E_L processes the image, obtaining a set of feature vector $\{z_{L,k} \in \mathbb{R}^d\}_{k=1}^K$. Then, each feature z_L is transformed through a matching mechanism, generating a token $q \in \mathbb{N}$ that corresponds to an item in the learnable low-quality VQ dictionary $\mathcal{C}_L = \{c_q \in \mathbb{R}^d\}_{q=1}^N$.

Visual Tokenizer. Tokenization is the process of dividing the input face into smaller units, *i.e.*, tokens. In our framework, the visual tokenizer maps the input face to categories in the low-quality VQ dictionary:

$$\mathcal{M} \circ E_L : \mathbb{R}^{H \times W \times 3} \rightarrow \mathbb{N}^K. \quad (5)$$

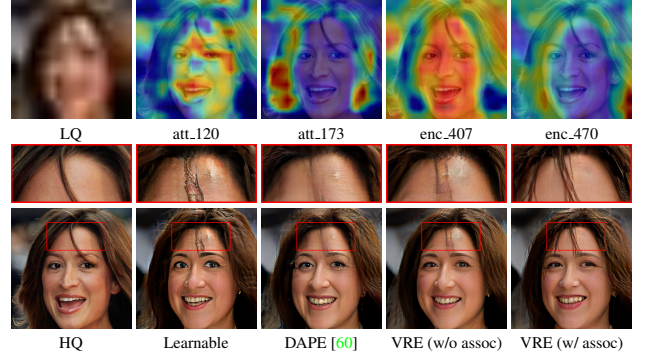


Figure 4. Attention maps of VRE and visual comparison of prompt embedding generation. We use CelebA-Test 0262 as an example.

For an LQ face denoted as I_L , we apply the VAE encoder E_L followed by the matching function \mathcal{M} to obtain the token set $\mathbf{Q}_L = \mathcal{M}(E_L(I_L))$. The token set \mathbf{Q}_L represents the predicted categories corresponding to LQ face.

VQ Embedder. The VQ embedder processes the token set by retrieving the corresponding items from the VQ dictionary. Specifically, for each image token q at position k , the embedder uses q as an index to access the dictionary item:

$$z_k = \text{dict}(q), \quad q \in \mathbf{Q}_L, \quad (6)$$

where z_k represents the k -th element of the visual prompt.

Unlike using image-to-tag models [39, 73] to generate tags as textual prompts, VRE directly tokenizes each face and converts the tokens into embeddings. This approach eliminates the information loss during the image-tag-embedding process. As illustrated in Fig. 4, VRE shows a strong recovery capacity. To study the working mechanism of VRE, we visualize the weight matrix of the final self-attention layer and the latent vector output by the VRE encoder. They are labeled as “att” and “enc” in the figure captions, respectively. The visualizations clearly indicate that the VRE focuses on both facial and nonfacial features. In summary, we can embed the LQ face I_L using VRE to obtain the visual prompt $p_L = \text{VRE}(I_L)$.

We construct two VQ dictionaries corresponding to the HQ and LQ image categories and train VQVAE using vector quantization [37] with self-reconstruction. Following VQGAN [12], we use GAN loss to promote extracting real-world features over noise. However, the LQ encoder sometimes focuses on meaningless categories due to strong degradation. Thus, we employ an alignment training strategy inspired by the CLIP model [39] to align the categories between LQ and HQ faces. By enhancing the diagonal correlation within VQ dictionaries, we could guide the LQ encoder to align its attention with the HQ encoder.

Training Objectives. We divide the loss functions into two parts. The first is a series of losses designed specifically for training the VQ dictionary, and the second is for association. Following previous works [16, 57, 74], we incorporate four types of losses during training. Three of them

are image restoration losses, *i.e.*, absolute differences \mathcal{L}_1 , perceptual function \mathcal{L}_{per} [21, 72], and discriminative loss \mathcal{L}_{dis} [20]). Since the VQ is non-differentiable, we adopt a classic quantization loss \mathcal{L}_{VQ} [2, 12, 37] additionally.

$$\begin{aligned}\mathcal{L}_1 &= \|I_h - I_h^{\text{rec}}\|_1, \mathcal{L}_{\text{per}} = \|\Phi(I_h) - \Phi(I_h^{\text{rec}})\|_2^2, \\ \mathcal{L}_{\text{dis}} &= [\log D(I_h) + \log(1 - D(I_h^{\text{rec}}))], \\ \mathcal{L}_{\text{VQ}} &= \|\text{sg}(Z_h) - Z_h^c\|_2^2 + \beta \|Z_h - \text{sg}(Z_h^c)\|_2^2.\end{aligned}\quad (7)$$

Here, $\Phi(\cdot)$ represents the feature extractor of VGG19 [45], D is a patch-based discriminator [20], and $\text{sg}(\cdot)$ denotes the stop-gradient operation. β is set to 0.25.

The combined loss \mathcal{L}_{VQ} is then defined as

$$\mathcal{L}_{\text{VQ}} = \mathcal{L}_1 + \lambda_{\text{per}} \cdot \mathcal{L}_{\text{per}} + \lambda_{\text{dis}} \cdot \mathcal{L}_{\text{dis}} + \mathcal{L}_{\text{VQ}}, \quad (8)$$

where we set $\lambda_{\text{per}} = 1.0$ and $\lambda_{\text{dis}} = 0.8$ in this setup.

Furthermore, we employ the cross-entropy loss introduced by DAEFR [51] to enhance the correlation between the HQ and LQ features. The similarity matrix $M_{\text{assoc}} \in \mathbb{R}^{K \times K}$ is constructed from the encoded feature z_H and z_L . We define the similarity score along the HQ axis of M_{assoc} as $p_{i,j}^h$, and along the LQ axis as $p_{i,j}^l$. The cross-entropy losses are then defined as

$$\begin{aligned}\mathcal{L}_{\text{CE}}^H &= -\frac{1}{K} \sum_{i=1}^K \sum_{j=1}^K y_{i,j} \log(p_{i,j}^h), \\ \mathcal{L}_{\text{CE}}^L &= -\frac{1}{K} \sum_{i=1}^K \sum_{j=1}^K y_{i,j} \log(p_{i,j}^l),\end{aligned}\quad (9)$$

where $y_{i,j}$ represents the ground truth label. The final target for the feature association component is then defined as

$$\mathcal{L}_{\text{assoc}} = (\mathcal{L}_{\text{CE}}^H + \mathcal{L}_{\text{CE}}^L) / 2. \quad (10)$$

The overall loss function for training the VRE at this stage can be expressed as

$$\mathcal{L}_{\text{total}} = \mathcal{L}_{\text{VQ}} + \lambda_{\text{assoc}} \cdot \mathcal{L}_{\text{assoc}}, \quad (11)$$

where λ_{assoc} is set to 0 for the initial epochs, and subsequently adjusted to 1 for the remaining epochs.

3.3. Stage 2. Realistic Face Alignment

Face restoration presents unique challenges and higher demands than general image restoration, as humans are exceptionally familiar with and sensitive to faces. Even minor inconsistencies or unnatural details in a generated face image are immediately noticeable (see Fig. 1), often resulting in an unrealistic appearance overall.

To ensure highly realistic face restoration, we design a series of losses aimed at guiding the model to generate globally harmonious and locally coherent face images. These carefully crafted losses play a key role in achieving high fidelity and visual authenticity. The overall loss function for the generator is defined as

$$\begin{aligned}\mathcal{L}_{\text{gen}} &= \lambda_{\text{dis}} \cdot \mathcal{L}_{\mathcal{G}}(z_H, \hat{z}_H) + \lambda_{\text{ID}} \cdot \mathcal{L}_{\text{ID}}(I_H, \hat{I}_H) \\ &+ \lambda_{\text{per}} \cdot \mathcal{L}_{\text{EA-DISTS}}(I_H, \hat{I}_H) + \text{MSE}(I_H, \hat{I}_H).\end{aligned}\quad (12)$$

Facial Identity Loss. A key challenge in face restoration is how to match each LQ face to a real, unique face portrait. However, during reconstruction, the model often struggles to render ambiguous features, leading to disharmonious facial attributes in the generated images. Inspired by advancements in face recognition tasks [33, 42, 50], we introduce a facial identity loss, specifically designed for face restoration. This loss leverages a pretrained face recognition model to measure feature similarity between the generated face and the target HQ image. The facial identity loss helps to enhance both the overall harmony of the generated face and the precise alignment of facial features.

We utilize a pretrained ArcFace model [9] to encode both the generated and HQ faces into identity embeddings (IDs). The cosine similarity between these IDs is then computed and used as a loss to guide model training. Denote the facial feature extraction model as \mathcal{F} . The facial identity loss \mathcal{L}_{ID} can be defined as follows

$$\mathcal{L}_{\text{ID}} = 1 - \cos(\mathcal{F}(I_H), \mathcal{F}(\hat{I}_H)). \quad (13)$$

Perceptual Loss. Although LPIPS [72] is widely used for perceptual evaluation, it can sometimes introduce visible artifacts, especially in diffusion models. To alleviate this issue, we use DISTS [10] to better capture texture details. During the reconstruction of LQ faces, DISTS preserves texture details more effectively while maintaining perceptual similarity, particularly in areas like hair and skin.

In addition, the accurate generation of edge details is essential for achieving perceived sharpness in face restoration. Thus, following the practice in D³SR [28], we introduce an edge-aware DISTS (EA-DISTS) as our perceptual loss

$$\begin{aligned}\mathcal{L}_{\text{EA-DISTS}}(\hat{I}_H, I_H) &= \mathcal{L}_{\text{DISTS}}(\hat{I}_H, I_H) \\ &+ \mathcal{L}_{\text{DISTS}}(\mathcal{S}(\hat{I}_H), \mathcal{S}(I_H)),\end{aligned}\quad (14)$$

where $\mathcal{S}(\cdot)$ is the Sobel operator.

GAN Loss. OSD models face challenges in generating stable images, due to their limited computational capacity. Previous studies [56, 59] typically employ distillation techniques to transfer knowledge from multi-step diffusion models. However, these methods are restricted by the performance limitations of the teacher models.

As an alternative, we use a discriminative network to enhance the realism of generated faces. This approach provides greater flexibility and improves computational efficiency. The adversarial loss, used to update both the generator \mathcal{G}_{θ} and discriminator \mathcal{D}_{θ} , is defined as

$$\mathcal{L}_{\mathcal{G}} = -\mathbb{E}_t [\log \mathcal{D}_{\theta}(F(\hat{z}_H, t))], \quad (15)$$

$$\begin{aligned}\mathcal{L}_{\mathcal{D}} &= -\mathbb{E}_t [\log(1 - \mathcal{D}_{\theta}(F(\hat{z}_H, t)))] \\ &- \mathbb{E}_t [\log \mathcal{D}_{\theta}(F(z_H, t))],\end{aligned}\quad (16)$$

where z_H is the latent vector of HQ face, and $F(\cdot, t)$ denotes the forward diffusion process at timestep $t \in [0, T]$.

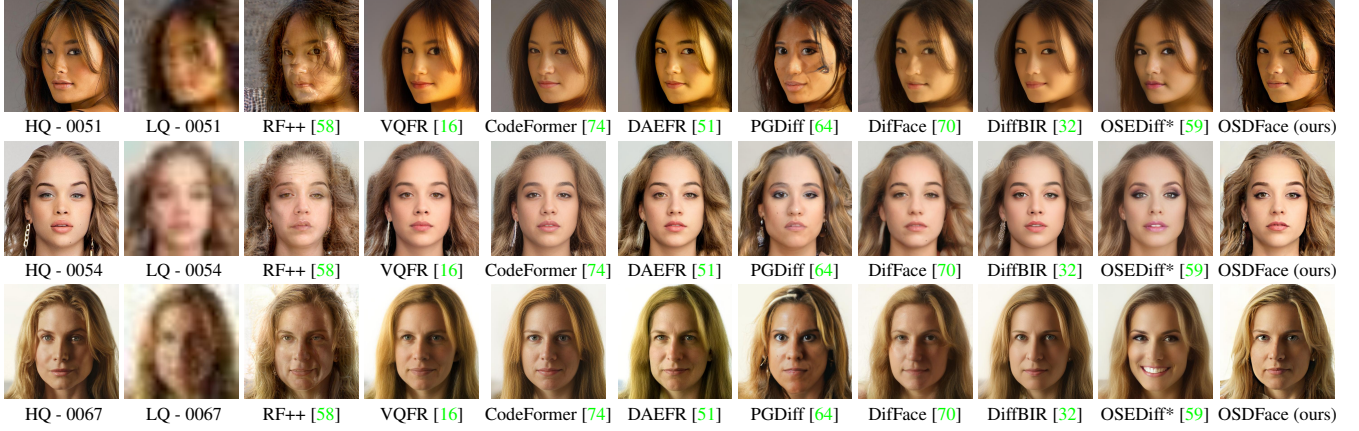


Figure 5. Visual comparison of the synthetic CelebA-Test dataset in challenging cases. Please zoom in for a better view.

Types	Methods	LPIPS↓	DISTS↓	MUSIQ↑	NIQE↓	Deg.↓	LMD↓	FID(FFHQ)	FID(HQ)↓
Non-Diffusion	RestoreFormer++ [58]	0.4535	0.2301	72.3612	3.9524	70.5083	8.8019	57.3723	72.7880
	VQFR [16]	0.3390	0.2131	73.2969	4.8374	62.2595	5.7297	58.1044	24.9093
	CodeFormer [74]	0.3412	0.2151	75.9432	4.5157	62.1972	5.3819	62.0280	26.8595
	DAEFR [51]	0.3580	0.2146	74.9853	4.4161	62.8184	5.6332	52.0341	26.0458
Multi-Step Diffusion	PGDiff [64] (s=1,000)	0.3866	0.1949	69.5676	4.0010	71.5996	7.3109	44.6258	26.3694
	DiffFace [70] (s=250)	0.3469	0.2126	66.7451	4.6381	63.4511	5.4759	49.8075	22.2370
	DiffBIR [32] (s=50)	0.3740	0.2340	75.6360	6.2801	61.0238	5.1042	71.7767	32.5109
One-Step Diffusion	OSediff [59] (s=1)	0.3306	0.2170	71.4674	5.1241	67.3904	6.4141	73.4843	37.2103
	OSediff* [59] (s=1)	0.3496	0.2200	69.9807	5.3280	67.4026	7.4082	81.3624	37.1309
	OSDFace (ours, s=1)	0.3365	0.1773	75.6398	3.8840	60.0708	5.2867	45.4150	17.0617

Table 1. Quantitative comparison on the synthetic CelebA-Test dataset with non-diffusion, multi-step diffusion, and one-step diffusion methods. The best and second best results are colored with red and blue.

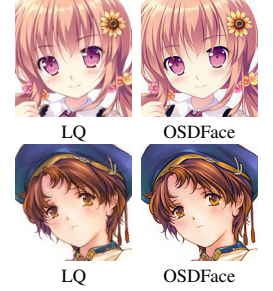


Figure 6. Zero-shot results of real-world cartoons.

4. Experiments

4.1. Experimental Settings

Training Datasets. Our model is trained on FFHQ [23] and its retouched version [43], containing 70,000 different high-quality face images. Images are resized to 512×512 pixels. Synthetic training data is generated using a dual-stage degradation model, with parameters following WaveFace [36]. This dual-stage degradation process closely aligns the synthetic data with real-world degradation scenarios, handling both mild and severe degradations.

Testing Datasets. We evaluate our method on the synthetic dataset CelebA-Test [22] from DAEFR [51] and three widely used real-world datasets: Wider-Test [74], LFW-Test [19], and WebPhoto-Test [54], following the settings in previous literature [16, 58, 74]. These datasets exhibit diverse and complex degradations. For example, the degradations in LFW-Test are relatively slight and regular, whereas those in Wider-Test are stronger.

Metrics. For the *Synthetic Dataset*, we employ LPIPS [72] and DISTS [10] as reference-based perceptual quality measures, together with MUSIQ [25] and NIQE [71] as no-reference image quality measures. To evaluate the distribution similarity between the ground truth and restored faces, we calculate FID [17] with both FFHQ and CelebA-Test HQ, showing the ability to recover “real” faces and HQ images. Following previous works [16, 51, 54], we use the em-

bedding angle of ArcFace [9], namely “Deg.”, and landmark distance, namely “LMD”, as additional identity and fidelity metrics. For the *Real-world Datasets*, we employ non-reference metrics, including FID (with FFHQ as reference), as well as CLIPQA [53], MANIQA [65], MUSIQ [25], and NIQE [71]. We utilize the evaluation codes provided by py-qa [5] and VQFR [16] for all metrics.

Implementation Details. In the first stage, we train the VRE using the Adam optimizer [27] with a learning rate of 1.44×10^{-4} and a batch size of 32. In our implementation, the input face image has dimensions of 512×512 , and the quantized feature map has dimensions of 256×512 after flattening. The VQ dictionaries contain $N=1,024$ code items, each with a channel size of 512. The HQ and LQ dictionaries are trained for 50 and 10 epochs, respectively. The association parameter λ_{assoc} is initially set to 0, followed by an additional 10 epochs with $\lambda_{\text{assoc}}=1$. The VRE is trained on 8 NVIDIA A800 GPUs.

In the second stage, our OSDFace is trained by the AdamW optimizer [34], with learning rate 1×10^{-4} and batch size 2 for both the generator and discriminator. The LoRA rank in the UNet is set to 16. The SD 2.1-base [1] serves as the pretrained OSD model, with the VRE used to construct the prompt embeddings. The setting of the discriminator is followed by D³SR [28], and the generator and discriminator are trained alternately. Training is performed for 150K iterations on 2 NVIDIA A6000 GPUs.

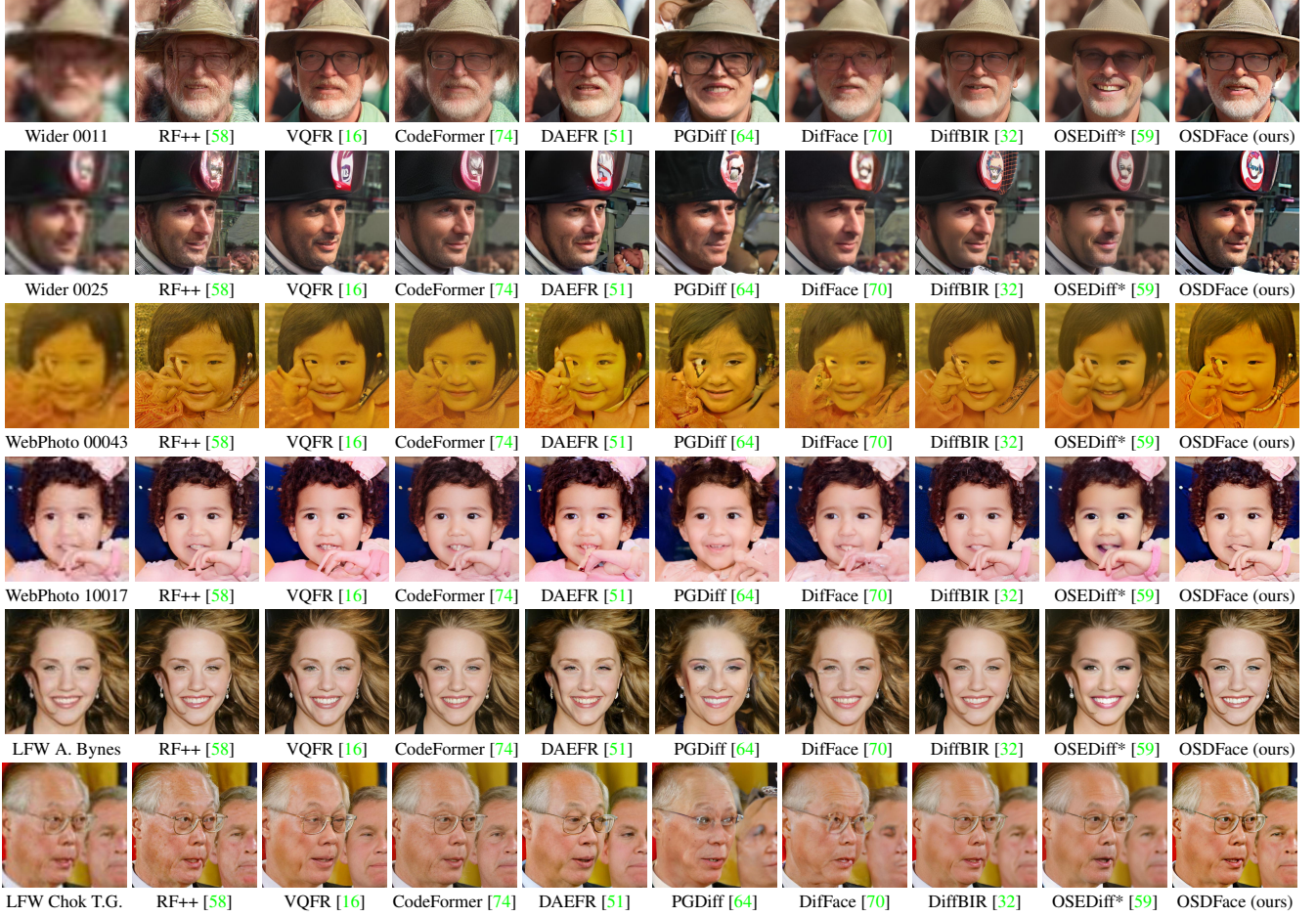


Figure 7. Visual comparison of the real-world datasets in challenging cases. Please zoom in for a better view.

Methods	Wider-Test					LFW-Test					WebPhoto-Test				
	C-IQA↑	M-IQA↑	MUSIQ↑	NIQE↓	FID↓	C-IQA↑	M-IQA↑	MUSIQ↑	NIQE↓	FID↓	C-IQA↑	M-IQA↑	MUSIQ↑	NIQE↓	FID↓
RestoreFormer++ [58]	0.7159	0.4767	71.332	3.7231	45.398	0.7024	0.5108	72.250	3.8434	50.253	0.6950	0.4902	71.484	4.0202	75.071
VQFR [16]	0.7069	0.5044	71.417	4.0357	37.866	0.7098	0.5339	74.385	3.8356	49.800	0.6769	0.4909	70.906	4.6095	84.776
CodeFormer [74]	0.6986	0.4958	73.406	4.1188	38.765	0.6890	0.5266	75.484	4.4377	52.341	0.6918	0.5034	74.001	4.6273	83.197
DAEFR [51]	0.6975	0.5205	74.143	3.5701	36.701	0.6964	0.5420	75.838	3.4788	47.527	0.6696	0.4934	72.698	3.9333	75.474
PGDiff [64] (s=1,000)	0.5824	0.4531	68.135	3.9315	35.862	0.5975	0.4858	71.244	4.0112	41.209	0.5653	0.4460	68.599	3.9930	86.954
DiffFace [70] (s=250)	0.5924	0.4299	64.907	4.2380	37.099	0.6075	0.4577	69.617	3.9016	46.127	0.5737	0.4189	65.116	4.2474	79.556
DiffBIR [32] (s=50)	0.8084	0.6625	75.321	5.5903	35.343	0.7948	0.6735	76.421	5.6782	40.320	0.7441	0.5839	72.272	6.0093	91.834
OSediff [59] (s=1)	0.6298	0.4951	70.559	4.9388	50.274	0.6326	0.5037	73.401	4.7196	57.800	0.6457	0.5108	72.593	5.2611	117.510
OSediff* [59] (s=1)	0.6193	0.4752	69.101	5.0869	47.883	0.6186	0.4879	71.707	4.8002	51.048	0.6254	0.4823	69.816	5.3253	109.236
OSDFace (ours, s=1)	0.7284	0.5229	74.601	3.7741	34.648	0.7203	0.5493	75.354	3.8710	44.629	0.7106	0.5162	73.935	3.9864	84.597

Table 2. Quantitative comparison on real-world datasets. C-IQA stands for CLIPQA, and M-IQA stands for MANIQA. The best and second best results are colored with red and blue. OSediff* is retrained on FFHQ dataset for reference.

Compared State-of-the-Art (SOTA) Methods. We compare OSDFace with several SOTA methods, including RestoreFormer++ [58], VQFR [16], CodeFormer [74], DAEFR [51], PGDiff [64], DiffFace [70] and DiffBIR [32]. We also provide the current SOTA OSD model OSediff [59], and retrain it on FFHQ [23], namely OSediff*.

4.2. Performance on Synthetic Data

Quantitative Results. The results in Tab. 1 demonstrate that OSDFace outperforms other methods in Deg., indicating better alignment with the ID features of HQ images. It

also achieves higher scores on LPIPS and DISTS, highlighting superior perceptual coherence and detail preservation. Performance in FID(HQ) shows that OSDFace effectively recovers the distribution of the original HQ dataset.

Qualitative Results. Visual comparisons in Fig. 5 illustrate that our method closely resembles real images. OSDFace enhances realism in elements such as earrings, eyelashes, eyebrows, hair strands, and subtle skin textures. Our approach restores hair most naturally, avoiding additional streaks or other regular textures, and maintains consistent hair color without random changes.

Methods	PGDiff [64]	DiffFace [70]	DiffBIR [32]	OSDiff [59]	OSDFace
Step	1,000	250	50	1	1
Time (s)	85.81	7.05	9.03	0.13	0.10
Param (M)	176.4	175.4	3,042	1,302	978.4
MACs (G)	480,997	18,682	189,208	2,269	2,132

Table 3. Complexity comparison during inference. All models are tested with an input image size of 512×512.

Methods	C-IQA↑	M-IQA↑	MUSIQ↑	NIQE↓	FID↓
Learnable	0.6714	0.5312	75.0339	4.0855	45.4041
DAPE [60]	0.6863	0.5622	74.8107	4.3801	45.9380
VRE (w/o assoc)	0.6791	0.5180	75.2328	3.8228	44.3360
VRE (w/ assoc)	0.6946	0.5356	75.2911	3.8793	41.9502

Table 4. Ablation study of prompt embedding generation. The best and second best results are colored with red and blue, respectively.

4.3. Performance on Real-world Data

Quantitative Results. In Tab. 2, we can see that OSDFace performs significantly better than another OSD method across all metrics. OSDFace outperforms non-diffusion models in most metrics. For multi-step diffusion models, we generally surpass PGDiff and DiffFace. For DiffBIR, we maintain a small gap and even exceed it in certain metrics.

Qualitative Results. Figure 7 visualizes representative images in three real-world datasets. Existing face restoration methods often emphasize facial features while overlooking the precise reconstruction of facial accessories like glasses, hair, hats, headwear, and background details. Some methods, especially DiffBIR [32], are over-smoothing and lack fine facial textures. OSDFace naturally and clearly restores multiple faces within a single image, showing its effectiveness for unaligned faces. OSDFace ensures high-fidelity restoration with balanced and consistent visual quality throughout the image. We also test its zero-shot ability on cartoon images in Fig. 6, using Anime Face Dataset [4].

4.4. Complexity Analysis.

Table 3 provides a detailed comparison of model complexity, including number of steps, inference time, parameter number, and multiply-accumulate operations (MACs) during inference. All evaluations are carried out on an NVIDIA A6000 GPU for consistency. **First**, by relying on one-step diffusion process, OSDFace significantly outperforms multi-step diffusion models in both inference time and MACs, demonstrating remarkable efficiency. **Furthermore**, OSDFace maintains an advantage over other OSD model. We do not incorporate text encoders (e.g., the DAPE used by OSDiff [59]), nor do we introduce additional modules that increase Stable Diffusion model complexity (e.g., the ControlNet used by DiffBIR [32]). Instead, we utilize a more efficient image encoder, VRE. **Consequently**, OSDFace achieves the lowest MACs count and fastest inference speed among all evaluated diffusion-based methods. Compared to the other OSD model, OSDiff [59], OSDFace demonstrates a 25% reduction in parameters and a 23% improvement in inference speed.

\mathcal{L}_{ID}	$\mathcal{L}_{EA-DISTS}$	\mathcal{L}_G	$\mathcal{L}_{EA-LPIPS}$	C-IQA↑	M-IQA↑	MUSIQ↑	NIQE↓	FID↓
	✓	✓		0.6724	0.5243	74.5986	4.0190	41.7842
✓		✓		0.6710	0.5387	74.1060	4.3223	55.1016
✓		✓	✓	0.6674	0.5470	75.2021	4.1484	46.1684
✓	✓			0.6590	0.5081	75.2336	3.9857	45.7834
✓	✓	✓		0.6946	0.5356	75.2911	3.8793	41.9502

Table 5. Ablation studies on different components. The best and second best results are colored with red and blue, respectively.

4.5. Ablation Studies

Visual Representation Embedder (VRE). We evaluated the impact of various prompt embedding generation methods on the training of OSDFace, including VRE, learnable prompt embeddings, and Degradation-Aware Prompt Extractor (DAPE) [60]. As shown in Tab. 4, the experimental results indicate that our method using VRE outperforms others across most metrics. As shown in Fig. 4, using VRE significantly enhances the facial details and the coherence of non-facial areas in the generated faces.

Furthermore, we trained the VRE using two approaches: with and without the HQ-LQ feature association loss, further validating the effectiveness of our method. As shown in the last two rows of Tab. 4, training with association loss achieves superior performance. This demonstrates that our VRE can extract valuable information from LQ images to guide face restoration effectively. **Notably**, with the inclusion of the feature association loss, the VRE gains the ability to identify and reconstruct certain HQ-like categories from LQ inputs, enhancing face restoration quality.

Realistic Face Alignment Loss. For the series of losses used in training the OSDFace, such as facial identity loss, EA-DISTS, and adversarial loss, we conducted extensive ablation studies. **Additionally**, we introduce the EA-LPIPS loss, defined similarly to EA-DISTS in Sec. 3.3. This loss first processes the image with the Sobel operator, followed by calculating the LPIPS loss. As shown in Tab. 5, the losses we utilized significantly contribute to model performance, with most metrics reaching the best scores.

5. Conclusion

We propose OSDFace, a high-speed diffusion model that enhances face image quality in one step. Our method bridges the gap between the powerful generative capabilities of text-to-image diffusion models and the specific requirements of face restoration. By introducing a visual prompt consistent with the model’s original conditional input, we effectively utilize prior information from the low-quality faces themselves. This enables the model to generate more realistic and high-fidelity face images. Our approach not only addresses the limitations of previous methods but also sets a new direction for incorporating visual priors into diffusion models for face restoration. Extensive experiments demonstrate that OSDFace achieves superior performance compared to recent state-of-the-art methods.

Acknowledgments

We thank the reviewers for their valuable feedback. This work was supported by the Shanghai Municipal Science and Technology Major Project (2021SHZDZX0102) and the Fundamental Research Funds for the Central Universities. Additionally, this work was supported in part by NSFC grant 2024YFC3017100, YDZX20253100004004, 62302299, Shanghai Science and Technology Development Funds under Grant 23YF1420500, and Huawei Explore X funds. Special thanks to Jianze Li for his technical support.

References

- [1] Stability AI. stabilityai/stable-diffusion-2-1-base. [Online]. Available: <https://huggingface.co/stabilityai/stable-diffusion-2-1-base>, 2022. 6
- [2] Yoshua Bengio, Nicholas Léonard, and Aaron Courville. Estimating or propagating gradients through stochastic neurons for conditional computation. *arXiv preprint arXiv:1308.3432*, 2013. 5
- [3] Kelvin CK Chan, Xintao Wang, Xiangyu Xu, Jinwei Gu, and Chen Change Loy. Glean: Generative latent bank for large-factor image super-resolution. In *CVPR*, 2021. 1
- [4] Brian Chao. Anime Face Dataset: a collection of high-quality anime faces., 2019. 8
- [5] Chaofeng Chen and Jiadi Mo. IQA-PyTorch: Pytorch toolbox for image quality assessment. [Online]. Available: <https://github.com/chaofengc/IQA-PyTorch>, 2022. 6
- [6] Chaofeng Chen, Xiaoming Li, Yang Lingbo, Xianhui Lin, Lei Zhang, and Kwan-Yee K. Wong. Progressive semantic-aware style transformation for blind face restoration. In *CVPR*, 2021. 1
- [7] Xiaoxu Chen, Jingfan Tan, Tao Wang, Kaihao Zhang, Wenhan Luo, and Xiaocun Cao. Towards real-world blind face restoration with generative diffusion prior. *arXiv preprint arXiv:2312.15736*, 2023. 1, 3
- [8] Yu Chen, Ying Tai, Xiaoming Liu, Chunhua Shen, and Jian Yang. Fsrnet: End-to-end learning face super-resolution with facial priors. In *CVPR*, 2018. 2
- [9] Jiankang Deng, Jia Guo, Xue Niannan, and Stefanos Zafeiriou. ArcFace: Additive angular margin loss for deep face recognition. In *CVPR*, 2019. 5, 6
- [10] Keyan Ding, Kede Ma, Shiqi Wang, and Eero P Simoncelli. Image quality assessment: Unifying structure and texture similarity. *IEEE TPAMI*, 2020. 5, 6
- [11] Berk Dogan, Shuhang Gu, and Radu Timofte. Exemplar guided face image super-resolution without facial landmarks. In *CVPRW*, 2019. 2
- [12] Patrick Esser, Robin Rombach, and Bjorn Ommer. Taming transformers for high-resolution image synthesis. In *CVPR*, 2021. 4, 5
- [13] Ben Fei, Zhaoyang Lyu, Liang Pan, Junzhe Zhang, Weidong Yang, Tianyue Luo, Bo Zhang, and Bo Dai. Generative diffusion prior for unified image restoration and enhancement. In *CVPR*, 2023. 3
- [14] Ian J. Goodfellow, Jean Pouget-Abadie, Mehdi Mirza, Bing Xu, David Warde-Farley, Sherjil Ozair, Aaron Courville, and Yoshua Bengio. Generative adversarial nets. In *NeurIPS*, 2014. 1
- [15] Jinjin Gu, Yujun Shen, and Bolei Zhou. Image processing using multi-code gan prior. In *CVPR*, 2020. 2
- [16] Yuchao Gu, Xintao Wang, Liangbin Xie, Chao Dong, Gen Li, Ying Shan, and Ming-Ming Cheng. VQFR: Blind face restoration with vector-quantized dictionary and parallel decoder. In *ECCV*, 2022. 3, 4, 6, 7
- [17] Martin Heusel, Hubert Ramsauer, Thomas Unterthiner, Bernhard Nessler, and Sepp Hochreiter. Gans trained by a two time-scale update rule converge to a local nash equilibrium. In *NeurIPS*, 2017. 6
- [18] Jonathan Ho, Ajay Jain, and Pieter Abbeel. Denoising diffusion probabilistic models. In *NeurIPS*, 2020. 1
- [19] Gary B. Huang, Marwan Mattar, Tamara Berg, and Eric Learned-Miller. Labeled Faces in the Wild: A Database for Studying Face Recognition in Unconstrained Environments. In *Workshop on Faces in 'Real-Life' Images: Detection, Alignment, and Recognition*, 2008. 6
- [20] Phillip Isola, Jun-Yan Zhu, Tinghui Zhou, and Alexei A. Efros. Image-to-image translation with conditional adversarial networks. In *CVPR*, 2017. 5
- [21] Justin Johnson, Alexandre Alahi, and Li Fei-Fei. Perceptual losses for real-time style transfer and super-resolution. In *ECCV*, 2016. 5
- [22] Tero Karras, Timo Aila, Samuli Laine, and Jaakko Lehtinen. Progressive growing of GANs for improved quality, stability, and variation. In *ICLR*, 2018. 6
- [23] Tero Karras, Samuli Laine, and Timo Aila. A style-based generator architecture for generative adversarial networks. In *CVPR*, 2019. 6, 7
- [24] Bahjat Kawar, Michael Elad, Stefano Ermon, and Jiaming Song. Denoising diffusion restoration models. In *NeurIPS*, 2022. 3
- [25] Junjie Ke, Qifei Wang, Yilin Wang, Peyman Milanfar, and Feng Yang. MUSIQ: Multi-scale Image Quality Transformer. In *ICCV*, 2021. 6
- [26] Deokyun Kim, Minseon Kim, Gihyun Kwon, and Dae-Shik Kim. Progressive face super-resolution via attention to facial landmark. In *BMVC*, 2019. 2
- [27] Diederik P Kingma and Jimmy Ba. Adam: A method for stochastic optimization. In *ICLR*, 2015. 6
- [28] Jianze Li, Jiezhong Cao, Zichen Zou, Xiongfei Su, Xin Yuan, Yulun Zhang, Yong Guo, and Xiaokang Yang. Unleashing the power of one-step diffusion based image super-resolution via a large-scale diffusion discriminator. *arXiv preprint arXiv:2410.04224*, 2024. 1, 3, 5, 6
- [29] Xiaoming Li, Ming Liu, Yuting Ye, Wangmeng Zuo, Liang Lin, and Ruigang Yang. Learning warped guidance for blind face restoration. In *ECCV*, 2018. 2
- [30] Xiaoming Li, Chaofeng Chen, Shangchen Zhou, Xianhui Lin, Wangmeng Zuo, and Lei Zhang. Blind face restoration via deep multi-scale component dictionaries. In *ECCV*, 2020.

- [31] Xiaoming Li, Wenyu Li, Dongwei Ren, Hongzhi Zhang, Meng Wang, and Wangmeng Zuo. Enhanced blind face restoration with multi-exemplar images and adaptive spatial feature fusion. In *CVPR*, 2020. 2
- [32] Xinqi Lin, Jingwen He, Ziyang Chen, Zhaoyang Lyu, Bo Dai, Fanghua Yu, Wanli Ouyang, Yu Qiao, and Chao Dong. Diff-BIR: Towards blind image restoration with generative diffusion prior. In *ECCV*, 2024. 1, 3, 6, 7, 8
- [33] Weiyang Liu, Yandong Wen, Zhiding Yu, Ming Li, Bhiksha Raj, and Le Song. SphereFace: Deep hypersphere embedding for face recognition. In *CVPR*, 2017. 5
- [34] Ilya Loshchilov and Frank Hutter. Decoupled weight decay regularization. In *ICLR*, 2019. 6
- [35] Sachit Menon, Alexandru Damian, Shijia Hu, Nikhil Ravi, and Cynthia Rudin. Pulse: Self-supervised photo upsampling via latent space exploration of generative models. In *CVPR*, 2020. 2
- [36] Yunqi Miao, Jiankang Deng, and Jungong Han. Waveface: Authentic face restoration with efficient frequency recovery. In *CVPR*, 2024. 1, 3, 6
- [37] Aaron Van Den Oord, Oriol Vinyals, et al. Neural discrete representation learning. In *NeurIPS*, 2017. 4, 5
- [38] Xinmin Qiu, Congying Han, Zicheng Zhang, Bonan Li, Tiande Guo, and Xuecheng Nie. Diffbfr: Bootstrapping diffusion model for blind face restoration. In *ACM MM*, 2023. 1, 3
- [39] A. Radford, J. Kim, C. Hallacy, A. Ramesh, G. Goh, S. Agarwal, A. Sastry, A. Askell, D. Mishkin, D. Clark, and G. Krueger. Learning transferable visual models from natural language supervision. In *ICML*, 2021. 4
- [40] Robin Rombach, Andreas Blattmann, Dominik Lorenz, Patrick Esser, and Bjorn Ommer. High-Resolution Image Synthesis with Latent Diffusion Models. In *CVPR*, 2022. 1, 3
- [41] Chitwan Saharia, William Chan, Saurabh Saxena, Lala Lit, Jay Whang, Emily Denton, Seyed Kamyar Seyed Ghasemipour, Burcu Karagol Ayan, S. Sara Mahdavi, Raphael Gontijo-Lopes, Tim Salimans, Jonathan Ho, David J Fleet, and Mohammad Norouzi. Photorealistic text-to-image diffusion models with deep language understanding. In *NeurIPS*, 2022. 1
- [42] Florian Schroff, Dmitry Kalenichenko, and James Philbin. FaceNet: A unified embedding for face recognition and clustering. In *CVPR*, 2015. 5
- [43] Alireza Shafaei, James J. Little, and Mark Schmidt. AutoRetouch: Automatic professional face retouching. In *WACV*, 2021. 6
- [44] Ziyi Shen, Wei-Sheng Lai, Tingfa Xu, Jan Kautz, and Ming-Hsuan Yang. Deep semantic face deblurring. In *CVPR*, 2018. 2
- [45] Karen Simonyan and Andrew Zisserman. Very deep convolutional networks for large-scale image recognition. In *ICLR*, 2015. 5
- [46] Jiaming Song, Chenlin Meng, and Stefano Ermon. Denoising diffusion implicit models. In *ICLR*, 2021. 1
- [47] Yang Song, Jascha Sohl-Dickstein, Diederik P Kingma, Abhishek Kumar, Stefano Ermon, and Ben Poole. Score-based generative modeling through stochastic differential equations. In *ICLR*, 2021. 1
- [48] Yang Song, Prafulla Dhariwal, Mark Chen, and Ilya Sutskever. Consistency models. In *ICML*, 2023. 4
- [49] Maitreya Suin and Rama Chellappa. CLR-Face: Conditional latent refinement for blind face restoration using score-based diffusion models. In *IJCAI*, 2024. 1, 2, 3
- [50] Yaniv Taigman, Ming Yang, Marc’Aurelio Ranzato, and Lior Wolf. DeepFace: Closing the gap to human-level performance in face verification. In *CVPR*, 2014. 5
- [51] Yu-Ju Tsai, Yu-Lun Liu, Lu Qi, Kelvin CK Chan, and Ming-Hsuan Yang. Dual associated encoder for face restoration. In *ICLR*, 2024. 1, 2, 3, 5, 6, 7
- [52] Ziyu Wan, Bo Zhang, Dongdong Chen, Pan Zhang, Dong Chen, Jing Liao, and Fang Wen. Bringing old photos back to life. In *CVPR*, 2020. 2
- [53] Jianyi Wang, Kelvin CK Chan, and Chen Change Loy. Exploring clip for assessing the look and feel of images. In *AAAI*, 2023. 6
- [54] Xintao Wang, Yu Li, Honglun Zhang, and Ying Shan. Towards real-world blind face restoration with generative facial prior. In *CVPR*, 2021. 1, 2, 6
- [55] Yinhuai Wang, Jiwen Yu, and Jian Zhang. Zero-shot image restoration using denoising diffusion null-space model. In *ICLR*, 2023. 3
- [56] Yufei Wang, Wenhan Yang, Xinyuan Chen, Yaohui Wang, Lanqing Guo, Lap-Pui Chau, Ziwei Liu, Yu Qiao, Alex C Kot, and Bihan Wen. Sinsr: diffusion-based image super-resolution in a single step. In *CVPR*, 2024. 3, 5
- [57] Zhouxia Wang, Jiawei Zhang, Runjian Chen, Wenping Wang, and Ping Luo. Restoreformer: High-quality blind face restoration from undegraded key-value pairs. In *CVPR*, 2022. 4
- [58] Zhouxia Wang, Jiawei Zhang, Tianshui Chen, Wenping Wang, and Ping Luo. Restoreformer++: Towards real-world blind face restoration from undegraded key-value pairs. *IEEE TPAMI*, 2023. 1, 3, 6, 7
- [59] Rongyuan Wu, Lingchen Sun, Zhiyuan Ma, and Lei Zhang. One-step effective diffusion network for real-world image super-resolution. In *NeurIPS*, 2024. 1, 2, 3, 5, 6, 7, 8
- [60] Rongyuan Wu, Tao Yang, Lingchen Sun, Zhengqiang Zhang, Shuai Li, and Lei Zhang. SeeSR: Towards semantics-aware real-world image super-resolution. In *CVPR*, 2024. 4, 8
- [61] Lianxin Xie, Csbingbing Zheng, Wen Xue, Le Jiang, Cheng Liu, Si Wu, and Hau San Wong. Learning degradation-unaware representation with prior-based latent transformations for blind face restoration. In *CVPR*, 2024. 1
- [62] Yichao Yan, Zanwei Zhou, Zi Wang, Jingnan Gao, and Xiaokang Yang. DialogueNeRF: towards realistic avatar face-to-face conversation video generation. *Visual Intelligence*, 2024. 1
- [63] Lingbo Yang, Shanshe Wang, Siwei Ma, Wen Gao, Chang Liu, Pan Wang, and Peiran Ren. Hifacegan: Face renovation via collaborative suppression and replenishment. In *ACM MM*, 2020. 2
- [64] Peiqing Yang, Shangchen Zhou, Qingyi Tao, and Chen Change Loy. PGDiff: Guiding diffusion models

- for versatile face restoration via partial guidance. In *NeurIPS*, 2023. 1, 2, 3, 6, 7, 8
- [65] Sidi Yang, Tianhe Wu, Shuwei Shi, Shanshan Lao, Yuan Gong, Mingdeng Cao, Jiahao Wang, and Yujiu Yang. MANIQA: Multi-dimension attention network for no-reference image quality assessment. In *CVPRW*, 2022. 6
- [66] Tao Yang, Peiran Ren, Xuansong Xie, and Lei Zhang. Gan prior embedded network for blind face restoration in the wild. In *CVPR*, 2021. 1
- [67] Tianwei Yin, Michaël Gharbi, Taesung Park, Richard Zhang, Eli Shechtman, Fredo Durand, and William T Freeman. Improved distribution matching distillation for fast image synthesis. In *NeurIPS*, 2024. 3
- [68] Tianwei Yin, Michaël Gharbi, Richard Zhang, Eli Shechtman, Frédo Durand, William T Freeman, and Taesung Park. One-step diffusion with distribution matching distillation. In *CVPR*, 2024. 3, 4
- [69] Xin Yu, Basura Fernando, Richard Hartley, and Fatih Porikli. Super-resolving very low-resolution face images with supplementary attributes. In *CVPR*, 2018. 2
- [70] Zongsheng Yue and Chen Change Loy. DiffFace: Blind Face Restoration with Diffused Error Contraction. *IEEE TPAMI*, 2024. 1, 3, 6, 7, 8
- [71] Lin Zhang, Lei Zhang, and Alan C. Bovik. A feature-enriched completely blind image quality evaluator. *IEEE TIP*, 2015. 6
- [72] Richard Zhang, Phillip Isola, Alexei A. Efros, Eli Shechtman, and Oliver Wang. The unreasonable effectiveness of deep features as a perceptual metric. In *CVPR*, 2018. 5, 6
- [73] Youcai Zhang, Xinyu Huang, Jinyu Ma, Zhaoyang Li, Zhaochuan Luo, Yanchun Xie, Yuzhuo Qin, Tong Luo, Yaqian Li, Shilong Liu, Yandong Guo, and Lei Zhang. Recognize Anything: A strong image tagging model. In *CVPR*, 2024. 4
- [74] Shangchen Zhou, Kelvin C.K. Chan, Chongyi Li, and Chen Change Loy. Towards robust blind face restoration with codebook lookup transformer. In *NeurIPS*, 2022. 1, 2, 3, 4, 6, 7

OSDFace: One-Step Diffusion Model for Face Restoration Supplementary Material

Jingkai Wang^{1*}, Jue Gong^{1*}, Lin Zhang¹, Zheng Chen¹
Xing Liu², Hong Gu², Yutong Liu^{1†}, Yulun Zhang^{1†}, Xiaokang Yang¹
¹Shanghai Jiao Tong University, ²vivo Mobile Communication Co., Ltd

A. Overall

This supplementary material provides additional results to support the main manuscript. First, in Section B, we analyze the parameter size of VRE and inference time. Next, in Section C, we present experiments that integrate VRE into OSDDiff [9]. These experiments demonstrate VRE’s strong image understanding capabilities. In Section D, we validate our method on downstream face recognition tasks. The results show that our method outperforms others when used as a pre-processing step. Additionally, we analysis the limitation and future work in Section E. Finally, in Section F, we provide more visual comparisons with state-of-the-art methods.

B. Parameters and Inference Time

Table 1 clearly shows that OSDFace achieves high inference speed and low computational cost compared to other one-step diffusion models. The VRE prompt embedder in OSDFace significantly reduces the parameter count and MACs. This reduction is notable when compared to the prompt embedder used in OSDDiff [9], *i.e.*, DAPE [10] with CLIP text encoder.

Additionally, generating text embeddings from input images does not conflict with generating latent vectors through a VAE encoder. Therefore, we can introduce a parallel mechanism that could speed up both OSDDiff [9] and OSDFace. Using parallel acceleration, our OSDFace could further reduce inference time by 14% on top of its fast performance. All tests are conducted on an NVIDIA A6000 GPU.

C. Integrating VRE into OSDDiff

The existing representative one-step diffusion (OSD) image restoration model, OSDDiff [9], does not focus on face restoration tasks. In order to assess its applicability to face restoration, we retrained it using the same dataset and experimental settings as OSDFace, resulting in OSDDiff*. Furthermore, we integrated the proposed VRE into OSDDiff*, creating the enhanced model OSDDiff*+VRE.

As shown in Tab. 2, Tab. 3, and Fig. 1, OSDDiff*+VRE

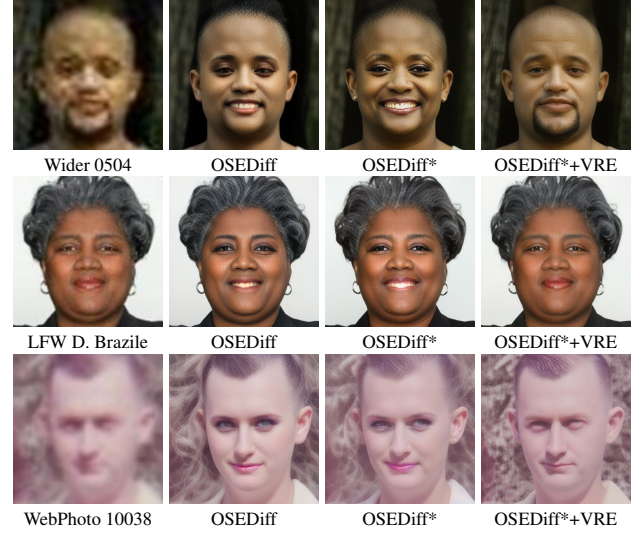


Figure 1. Visual comparisons of various versions of OSDDiff [9]. OSDDiff*+VRE shows enhanced visual quality.

Methods	Prompt Embedder		Inference Time (ms)	
	Param (M)	MACs (G)	Serialized	Parallelized
OSDDiff [9]	353.41	141.45	130.75	125.54
OSDFace (ours)	28.63	99.47	119.00	102.83

Table 1. Complexity comparison during inference. “parallelized” refers to the parallel execution of the prompt embedder and VAE encoder, while “serialized” denotes a fully sequential execution approach. We provide the number of parameters (Param), multiply-accumulate operations (MACs), and time during inference. All models are evaluated with 512×512 input image.

performs well in both quantitative metrics and visual quality. The incorporation of VRE significantly reduces information loss during the image-text-embedding process, ensuring more accurate data representation. Visual results indicate that OSDDiff*+VRE prevents common issues like gender misclassification and unwanted artifacts. Additionally, it reliably captures subtle facial expressions from the input images. Besides, the IQA metrics demonstrate a competitive advantage by consistently reducing the distribution differences from the reference data. These experimental results demonstrate that our proposed VRE substantially enhances face restoration performance, particularly when applied to OSD models.

*Equal contribution.

†Corresponding authors.

Methods	Wider-Test					LFW-Test					WebPhoto-Test				
	C-IQA↑	M-IQA↑	MUSIQ↑	NIQE↓	FID↓	C-IQA↑	M-IQA↑	MUSIQ↑	NIQE↓	FID↓	C-IQA↑	M-IQA↑	MUSIQ↑	NIQE↓	FID↓
OSDiff [9]	0.6298	0.4951	70.559	4.9388	50.274	0.6326	0.5037	73.401	4.7196	57.800	0.6457	0.5108	72.593	5.2611	117.510
OSDiff*	0.6193	0.4752	69.101	5.0869	47.883	0.6186	0.4879	71.707	4.8002	51.048	0.6254	0.4823	69.816	5.3253	109.236
OSDiff*+VRE	0.6637	0.4834	68.259	5.0490	41.490	0.6608	0.5015	70.826	4.8956	46.911	0.6410	0.4646	66.912	5.5233	95.566
OSDFace (ours)	0.7284	0.5229	74.601	3.7741	34.648	0.7203	0.5493	75.354	3.8710	44.629	0.7106	0.5162	73.935	3.9864	84.597

Table 2. Quantitative comparison on real-world datasets with one-step diffusion methods. C-IQA stands for CLIPQA, and M-IQA stands for MANIQA. The best and second best results are colored with red and blue, respectively.

Methods	LPIPS↓	DISTS↓	MUSIQ↑	NIQE↓	Deg.↓	LMD↓	FID(FFHQ)↓	FID(HQ)↓
OSDiff [9]	0.3306	0.2170	71.467	5.1241	67.390	6.4141	73.484	37.210
OSDiff*	0.3496	0.2200	69.981	5.3280	67.403	7.4082	81.362	37.131
OSDiff*+VRE	0.3368	0.2420	69.089	5.3241	63.758	6.5365	67.785	36.356
OSDFace (ours)	0.3365	0.1773	75.640	3.8840	60.071	5.2867	45.415	17.062

Table 3. Quantitative comparison on the synthetic CelebA-Test dataset with one-step diffusion methods. The best and second best results are colored with red and blue, respectively.

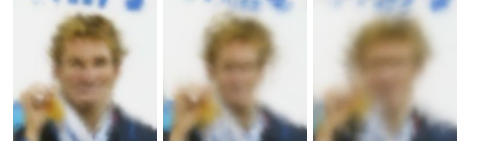


Figure 2. Visualization of the atmospheric turbulence [1] range from 20,000 to 40,000.

D. Validation on Face Recognition

Face restoration, as a fundamental low-level vision task, could enhance downstream face recognition tasks to achieve better performance. We use the LFW [4] dataset as a benchmark for comparison, which includes 3,000 positive pairs and 3,000 negative pairs. Following DAEFR [7], we evaluate the face recognition accuracy using the ArcFace [2] model under different degradation levels. Specifically, we employ unseen atmospheric turbulence degradation [1] to simulate diverse degradation levels, with propagation lengths ranging from 20,000 to 40,000, as illustrated in Fig. 2.

The experimental results in Fig. 3 demonstrate the superior performance of our method across various degradation levels. As degradation severity increases, our method significantly improves precision at the same recall level. The ROC curve shows that OSDFace makes fewer errors at specific true positive rates. Besides, OSDFace widens the gap between positive and negative predictions, thereby improving classifier performance. These findings indicate that our method provides substantial enhancements to downstream face recognition tasks.

E. Limitations and Future Work

We briefly analyze the limitations and future work. (1) Color shift: OSDFace sometimes over-enhances contrast or saturation in less degraded regions, causing color shifts in restored face images. Although AdaIN [5] can fix this during inference, we aim for an end-to-end, color shift-free restoration. Future work will explore content-aware color regularization to improve color preservation. (2) Texture in complex regions: OSDFace struggles with realistic skin textures and fine details in complex regions like limbs or fingers. This arises from the model’s focus on face features, with limited training data for non-facial parts with similar skin textures. Future work will explore semantic information extraction and domain-specific priors to improve the handling of these areas. (3) Generalization to low-degradation images: OSDFace was not trained on minimal degradation images, but still shows some generalization. However, finer skin texture restoration remains a focus, requiring higher resolution input and output faces, HD training data, and texture-sensitive architectures.

F. Additional Visual Comparisons

These comparisons demonstrate that our proposed OSDFace generates high-quality faces and effectively preserves identities, even with severely degraded input images. Compared to other methods, OSDFace more accurately recovers finer details and produces more realistic faces. To illustrate these advantages further, we select various representative images with unique characteristics, which can be regarded as different face categories. These images are briefly analyzed below.

Synthetic dataset. Visualized results are presented in Fig. 4, Fig. 5, and Fig. 6. Compared to other methods, OSDFace produces more natural-looking restorations with greater detail. This is especially evident in the hair, whether long, short, straight, or curly. Additionally, our method effectively restores occluded regions, such as an arm covering the mouth or bangs obscuring the eyes. For profile views, OSDFace naturally recovers facial contours. In some ground truth images with blurred backgrounds, OSDFace performs well, even achieving higher quality and greater detail than the original HQ images. In scenarios with complex backgrounds, many VQ-based methods, such as VQFR [3], CodeFormer [13], and DAEFR [7], fail to restore natural backgrounds. These methods often produce wallpaper-like outputs, exhibit color distortions, or even blend the person’s clothing with the background. In contrast, OSDFace, which combines VQ Dict and diffusion model, successfully generates harmonious faces.

Real-world dataset. More visual comparisons on real-world datasets are shown in Fig. 7, Fig. 8, Fig. 9, and Fig. 10. Our OSDFace demonstrates strong capabilities in detail generation and boundary distinction. Some images contain multiple closely positioned faces, such as image 0026 in the Wider-Test and Damon Stoudamire in the LFW-Test. Our method successfully restores each individual face. In Wider 0003, only OSDFace successfully generates complete glasses and clearly separates the arm from the face. For faces with varying skin tones, our method consistently maintains the realism of the images. Furthermore, our approach accurately restores facial accessories, including patterns on hats (Wider 0026), bandages (Daniel Osorno in LFW-Test), and earrings (Wider 0173). In old photo restoration scenarios, our OSDFace also effectively handles unknown degradations.

References

- [1] Nicholas Chimitt and Stanley H Chan. Simulating anisoplanatic turbulence by sampling intermodal and spatially correlated zernike coefficients. *Optical Engineering*, 2020. 2
- [2] Jiankang Deng, Jia Guo, Xue Niannan, and Stefanos Zafeiriou. ArcFace: Additive angular margin loss for deep face recognition. In *CVPR*, 2019. 2, 4
- [3] Yuchao Gu, Xintao Wang, Liangbin Xie, Chao Dong, Gen Li, Ying Shan, and Ming-Ming Cheng. VQFR: Blind face restoration with vector-quantized dictionary and parallel decoder. In *ECCV*, 2022. 2, 5, 6, 7, 8, 9, 10, 11
- [4] Gary B. Huang, Marwan Mattar, Tamara Berg, and Eric Learned-Miller. Labeled Faces in the Wild: A Database for Studying Face Recognition in Unconstrained Environments. In *Workshop on Faces in 'Real-Life' Images: Detection, Alignment, and Recognition*, 2008. 2, 4
- [5] Xun Huang and Serge Belongie. Arbitrary style transfer in real-time with adaptive instance normalization. In *ICCV*, 2017. 2
- [6] Xinqi Lin, Jingwen He, Ziyang Chen, Zhaoyang Lyu, Bo Dai, Fanghua Yu, Wanli Ouyang, Yu Qiao, and Chao Dong. Diff-BIR: Towards blind image restoration with generative diffusion prior. In *ECCV*, 2024. 5, 6, 7, 8, 9, 10, 11
- [7] Yu-Ju Tsai, Yu-Lun Liu, Lu Qi, Kelvin CK Chan, and Ming-Hsuan Yang. Dual associated encoder for face restoration. In *ICLR*, 2024. 2, 5, 6, 7, 8, 9, 10, 11
- [8] Zhouxia Wang, Jiawei Zhang, Tianshui Chen, Wenping Wang, and Ping Luo. Restoreformer++: Towards real-world blind face restoration from undegraded key-value pairs. *IEEE TPAMI*, 2023. 5, 6, 7, 8, 9, 10, 11
- [9] Rongyuan Wu, Lingchen Sun, Zhiyuan Ma, and Lei Zhang. One-step effective diffusion network for real-world image super-resolution. In *NeurIPS*, 2024. 1, 2, 5, 6, 7, 8, 9, 10, 11
- [10] Rongyuan Wu, Tao Yang, Lingchen Sun, Zhengqiang Zhang, Shuai Li, and Lei Zhang. SeeSR: Towards semantics-aware real-world image super-resolution. In *CVPR*, 2024. 1
- [11] Peiqing Yang, Shangchen Zhou, Qingyi Tao, and Chen Change Loy. PGDiff: Guiding diffusion models for versatile face restoration via partial guidance. In *NeurIPS*, 2023. 5, 6, 7, 8, 9, 10, 11
- [12] Zongsheng Yue and Chen Change Loy. DiffFace: Blind Face Restoration with Diffused Error Contraction. *IEEE TPAMI*, 2024. 5, 6, 7, 8, 9, 10, 11
- [13] Shangchen Zhou, Kelvin C.K. Chan, Chongyi Li, and Chen Change Loy. Towards robust blind face restoration with codebook lookup transformer. In *NeurIPS*, 2022. 2, 5, 6, 7, 8, 9, 10, 11

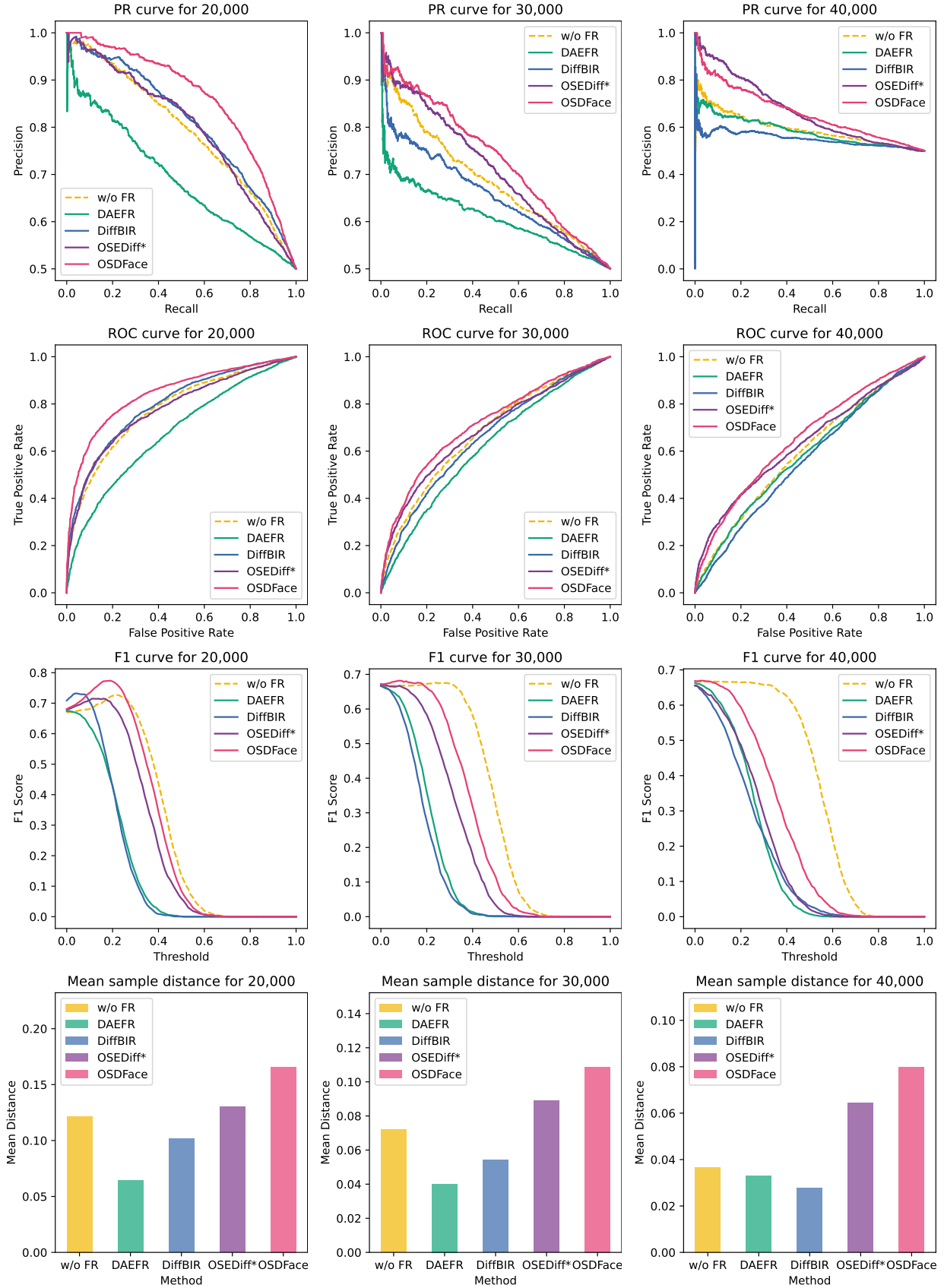


Figure 3. Quantitative results on the LFW dataset [4] for face recognition using the official ArcFace [2] MS1MV3 R50 model. The evaluated metrics include precision-recall (PR) curves, receiver operating characteristic (ROC) curves, F1 scores, and mean sample distance histograms. The mean sample distance is defined as the difference between the average cosine similarity of predicted positive pairs and predicted negative pairs. “w/o FR” refers to the absence of the face restoration process. Atmospheric turbulence parameters range from 20,000 to 40,000.

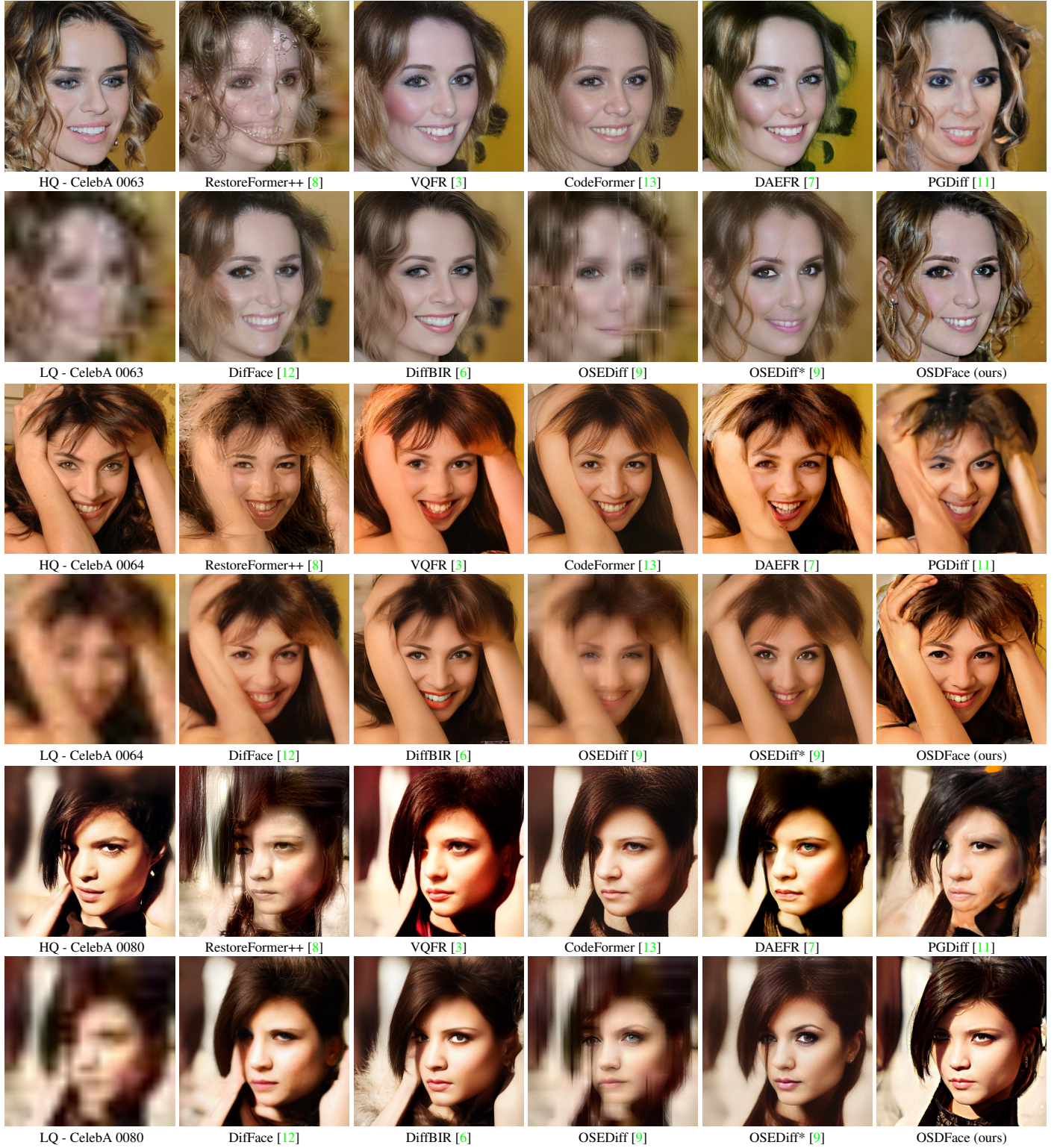


Figure 4. More visual comparison of the synthetic CelebA-Test dataset in challenging cases. Please zoom in for a better view.

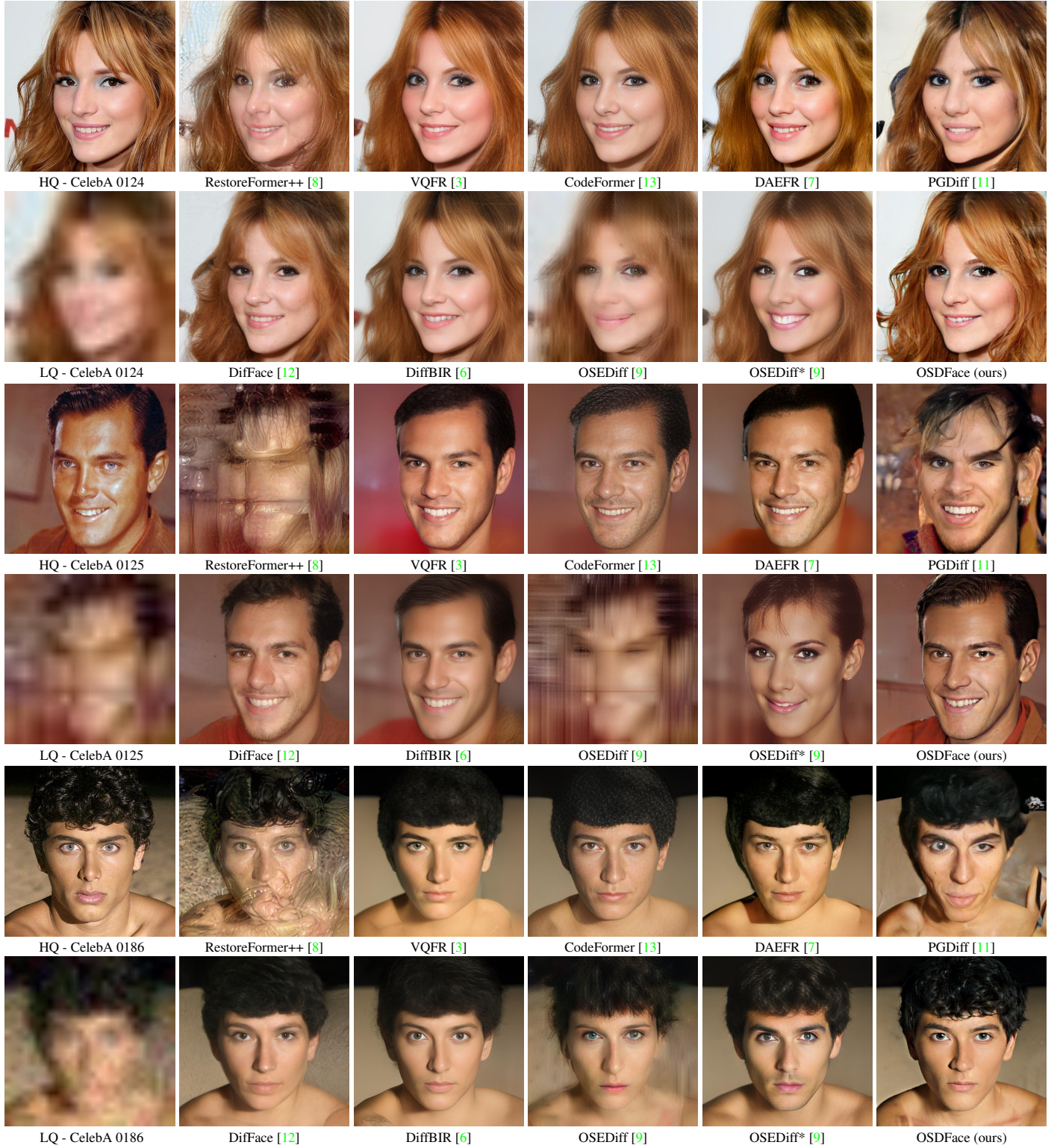


Figure 5. More visual comparison of the synthetic CelebA-Test dataset in challenging cases. Please zoom in for a better view.

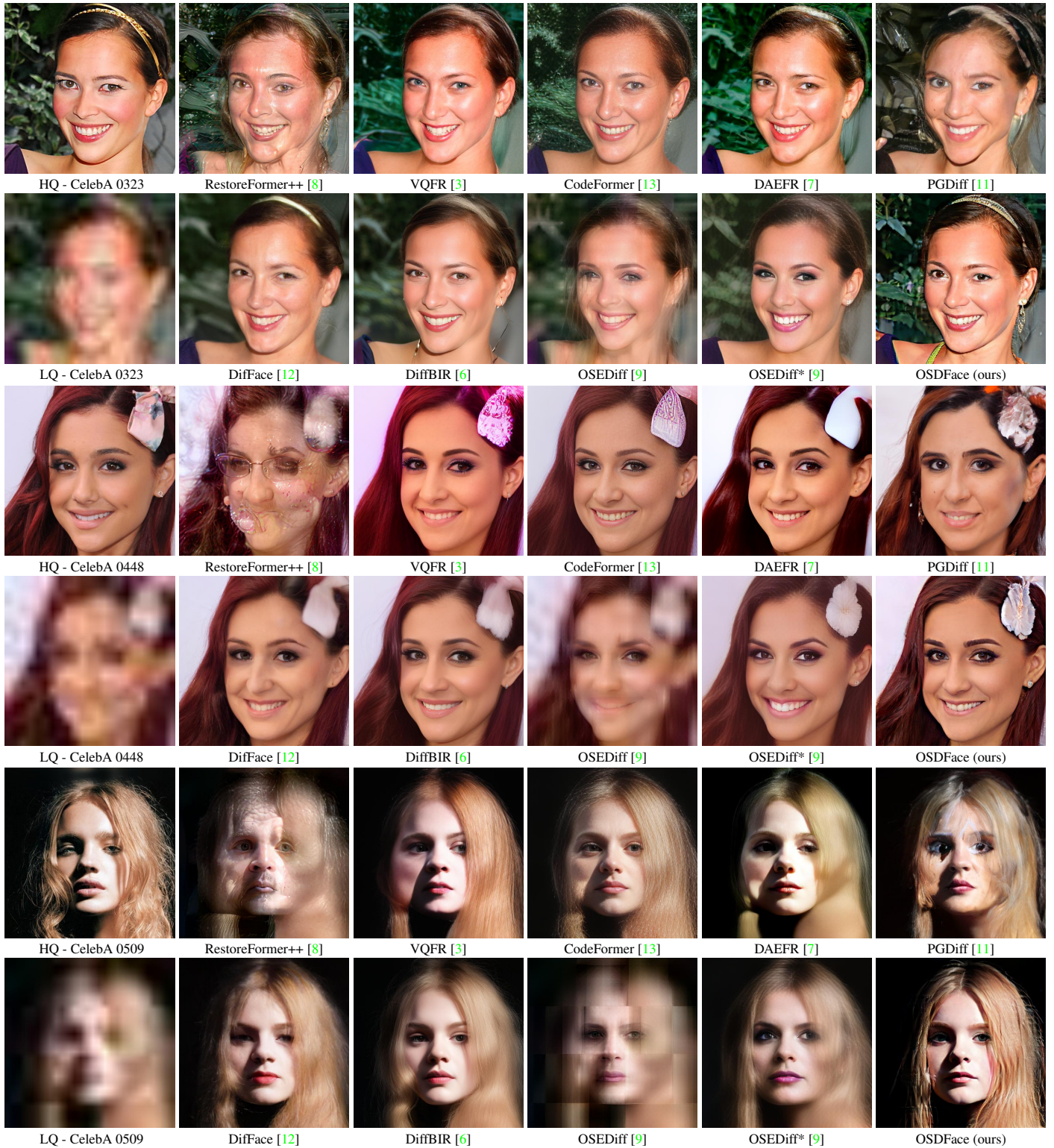


Figure 6. More visual comparison of the synthetic CelebA-Test dataset in challenging cases. Please zoom in for a better view.

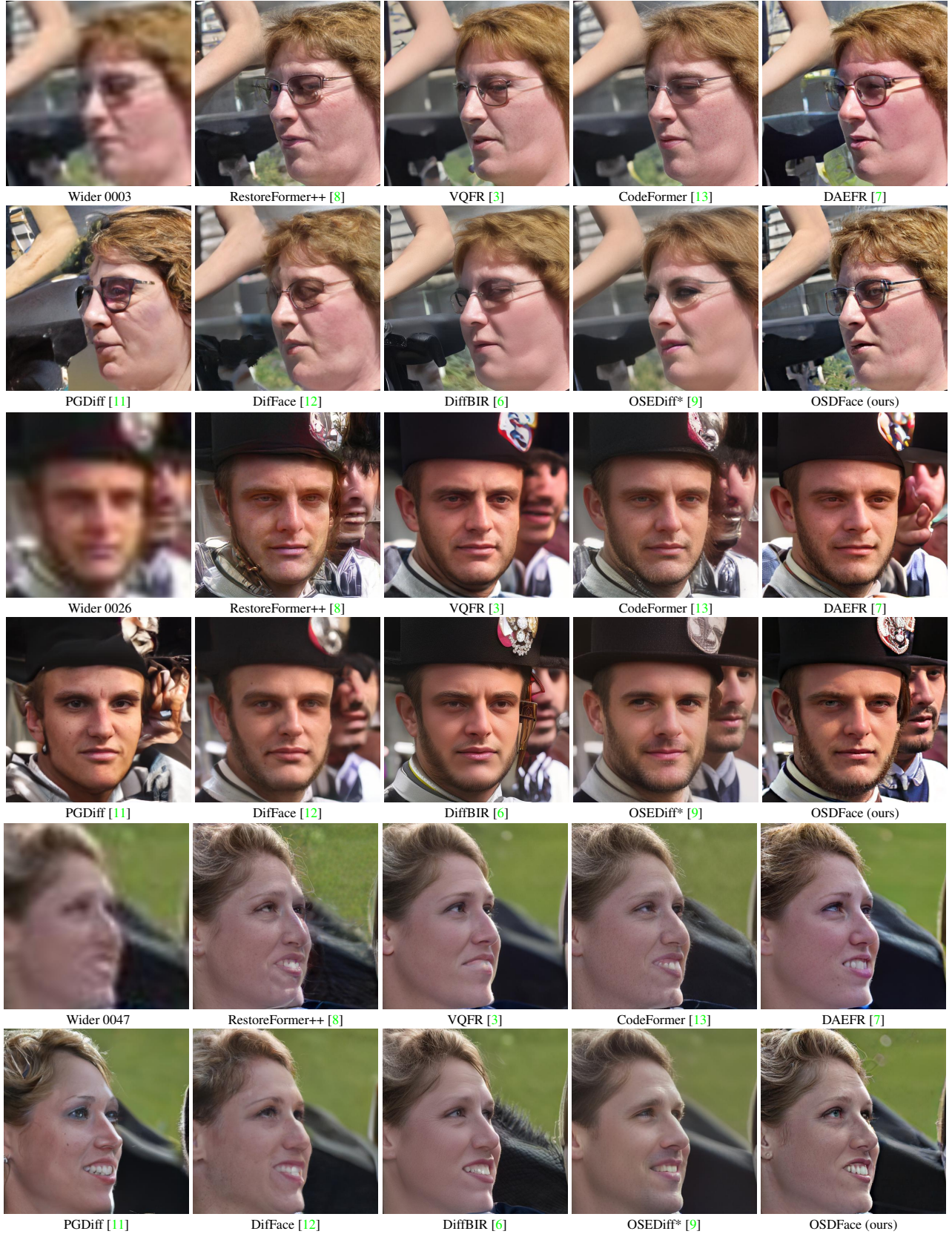


Figure 7. More visual comparison of the real-world Wider-Test dataset in challenging cases. Please zoom in for a better view.

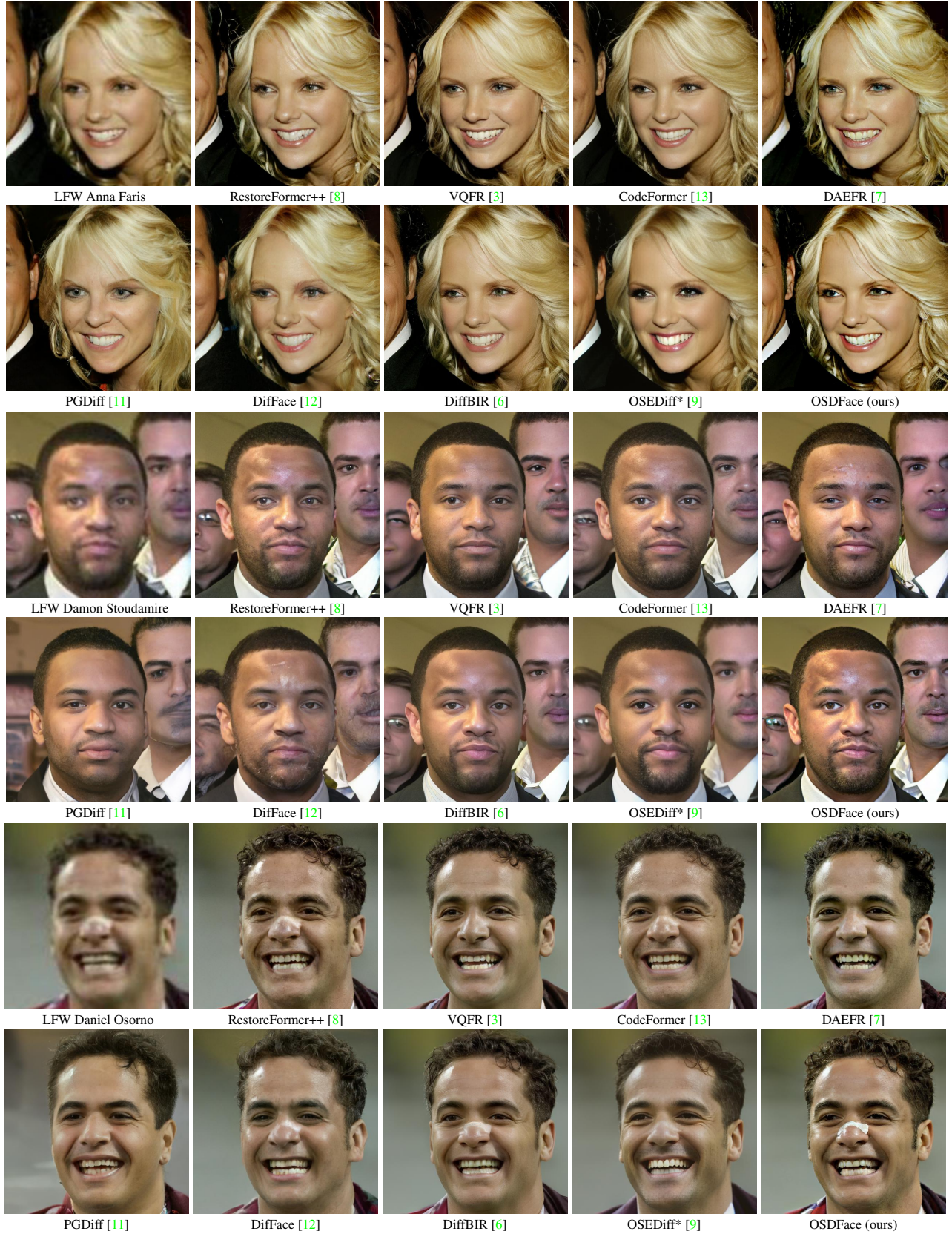


Figure 8. More visual comparison of the real-world LFW-Test dataset in challenging cases. Please zoom in for a better view.



Figure 9. More visual comparison of the real-world WebPhoto-Test dataset in challenging cases. Please zoom in for a better view.

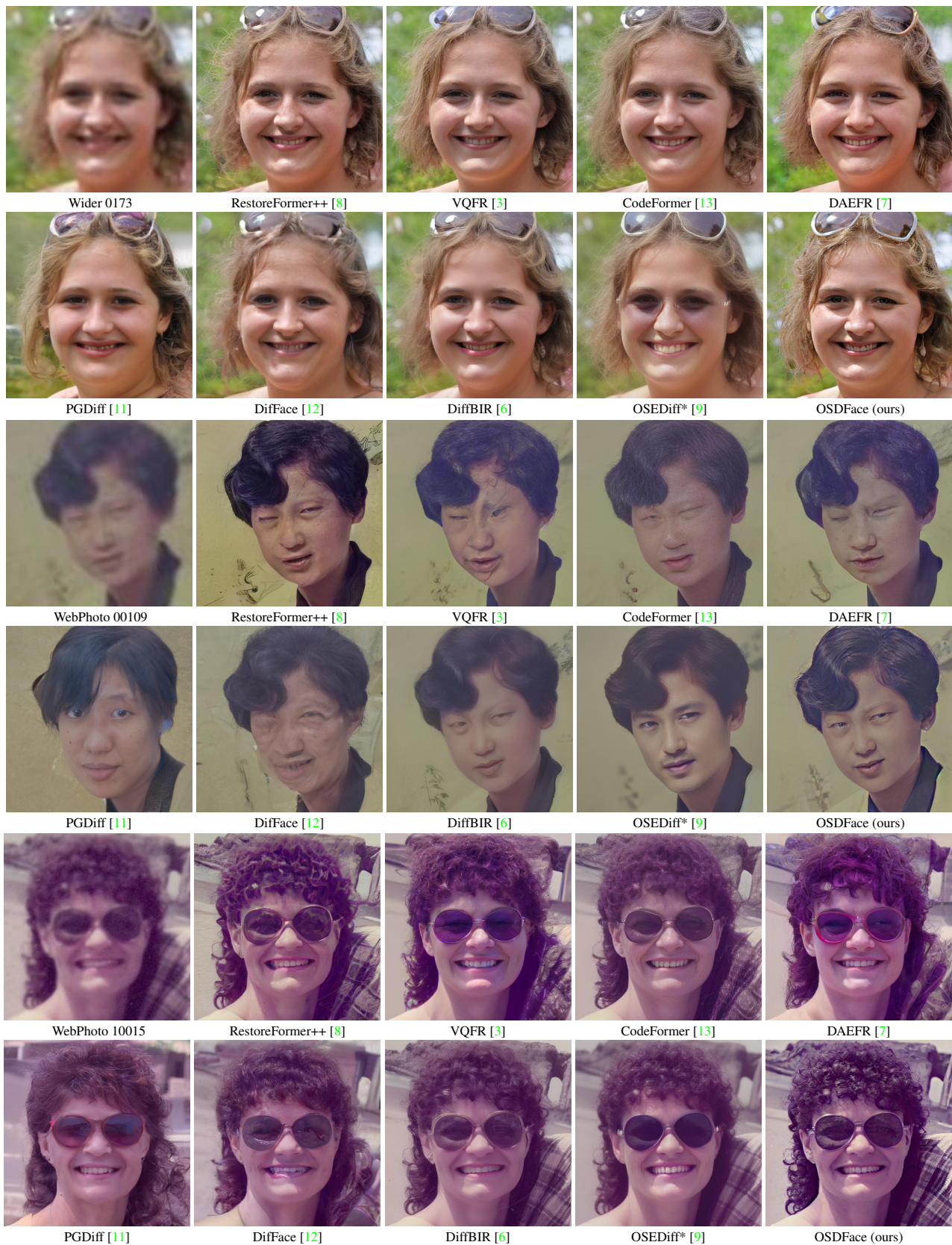


Figure 10. More visual comparison of the real-world datasets in challenging cases. Please zoom in for a better view.